P2F.15 On Causes of Rainband Breaking for Asymmetric Precipitation in Typhoon Haitang (2005) before and after its landfall

Ding Zhiying, Wang Yong Wang Yongqing

Pacific Typhoon Research Center, KLME, Nanjing University of Information Science & Technology

Nanjing , China, 210044，Email: lvran0122@163.com

Abstract Using WRF (Weather Research Forecast) model, analysis and simulation are performed of the rainband change around the time when the 2005 typhoon *Haitang（2005）* landed on China, indicating that the breaking may occur over land and ocean, thereby leading to more distinct asymmetric precipitation, and the breaking relates not only to topography but to interactions between the typhoon and midlatitude systems at higher levels; around the time of landfall the 200 hPa South-Asian high divergent flows combined with divergent air outside the typhoon travel towards a weak inverted trough in the northwest part of the tempest and the mid- and low-level divergence fields on the west and northwest side of the typhoon center are maintained steadily, thus intensifying the high-level cyclonic flows, associated with which part of positive vorticity rotates counterclockwise together with currents, traveling stepwise into the vorticity zone in the vicinity of the typhoon core, thereby forming a vorticity transfer belt in 22~25^{0}N that extends to the eastern part of the storm, where the high-level vorticity band shows subsidence that prevents rainfall from development, resulting in the rainbelt breaking, which is the principal cause of asymmetric precipitation occurrence. The banded vorticity of the 0505 tropical cyclone at high levels migrating into its outer region cause further amplification of cyclonic circulation in the western part and of positive vorlicity transfer into the typhoon such that the rainband breaking is more distinct.

Keywords: Typhoon；Rainband；Asymmetric Precipitation；WRF；Interaction

1. INTRODUTCION

Typhoon (or tropical cyclone, TC) rainfall tends to be asymmetric, particularly around the time of its landfall the asymmetric precipitation is perceptible, whose causes are being actively investigated. Many studies are devoted to the impacts of different-scale interactions upon such rainfall (Tao et al., 1994; Chen and Meng, 2001) and a large number of researches are concerned with relationships of interactions of mid-level subtropical high and typhoon to precipitation (e.g., Nikaidon, 1989; Rodgers et al., 1994; Ren et al., 2007). Besides, the matching of high- and lower-level weather systems in relation to rainfall has been receiving more and more attention from scientists. As indicated in Zhu et al. (2003), for example, based on their simulations of the evolution of the 1998 hurricane Bonnie eye wall and its strength, its amplification bore a relation not only to low-level vapor supply and of warm underlying surface but to the approaching northwesterlies at high levels when the hurricane was deepening, thus producing mass convergence and subsidence making for air warming and drying, which suppress the deep convection happening in the western half circle of Bonnie, which caused asymmetry of part of the eye wall, cloud and precipitation as well as the eastward tilt of the wall and storm center. That analysis demonstrated substantial influence of the variation in high-level systems on the hurricane's structure and asymmetric precipitation. In their researches into effects of high-level systems upon typhoon precipitation, Chinese investigators have focus on the rainfall related to a TC landing far away (Chen and Ding, 2000; Sun et al., 2006). The summertime high levels over China are under the control of the south Asian high but generally TC are reflected weakly in the higher troposphere. However, a typhoon, when approaching the land, has its high-level portion prone to the effect of midlatitude systems and variations in the high-level circulations are likely to affect the distribution of TC rainbelts. But how do the high-level systems impact the pattern of precipitation around the time when the TC makes landfall? In particular, the research efforts are fewer as regards the effects of interactions between the midlatitude systems and typhoon circulation at higher levels upon asymmetric rainfall happening before and after its landfall. For

Corresponding author address: Prof. Zhiying D.,Dept. of Atmospheric Sciences, University of Information Science & Technology ,Nanjing , China, 210044，e-mail: lvran0122@163.com

this reason, study is undertaken of the variation in the *Haitang* rainband and interactions between the high-level midlatitude systems and the 0505 TC in the framework of WRF model-given simulations in an attempt to find out the causes of asymmetric precipitation occurring around the time when the TC landed.

2. DATA AND INTRODUTCION TO THE MODEL

Data were NCEP reanalysis at $1^0 \times 1^0$ resolution utilized with the meso non-static WRF model to make simulation of the *Haitang* - caused rainstorm over the southeastern seaboards of southern and central Zhejiang province for July 19/0000 ~ 20/0000 UTC, 2005 in conjunction with the control and reduced-terrain height sensitivity experiments conducted. The model structure, physics and scheme are presented as follows.

1) Dual meshes were employed, with the coarse (fine) mesh gridpoints arriving at 181×161 (169×196) at 18 (6) km spacing;
2) The model top was at 50 hPa, separated by 28 levels in vertical;
3) The schemes were the versions of cumulus convection parameterization; with Kain/Fritsch (Grell) scheme for the coarse (fine) mesh;
4) The integration duration covered 19/0000 ~ 20/0000 UTC, July of 2005, with the output taken on an hourly basis and the timestep of 90 sec.

For the sensitivity run the terrain height was reduced below 200 m over 23~29^{0}N, east of 110^{0}E (figure not shown), otherwise as in the control experiment. Unless stated otherwise, the analysis was made of results from the control experiment.

In situ 1-h rainfall rates taken at 3-h intervals came from the automatic meteorological stations, with reference to TRMM gridded precipitation at 25×25 km spacing.

3. SIMULATED RAINFALL AND TYPHOON TRACK COMPARED WITH OBSERVATIONS

Comparison between measured and fine-mesh simulated 24-hr precipitation starting from 0000 UTC, July 19 (Figs.1a, b) yields that two emulated >300 mm centers (28.2^{0}N, 121^{0}E, and 27.2^{0}N, 120^{0}E) are in rough coincidence with the in situ observed counterparts (27.5^{0}N, 120.5^{0}E, and 28.2^{0}N, 121^{0}E). The simulated rainfall in 27.2^{0}N, 120^{0}E (28.2^{0}N, 121^{0}E) happened mainly over 0000~0900 (0500~1600) UTC, July 19 while the measured precipitation occurred in 27.5^{0}N, 120.5^{0}E (28.2^{0}N, 121^{0}E) largely over 0000~0600 (0600~1800) UTC, thus showing the rainfall time interval to be close of the simulations to observations. The modeled precipitation was slightly smaller compared to the measurement in the north while the simulation and observation were comparable to each other in the south.

No rainfall records were available over the sea for testing so that the 1-hr gridded data provided by TRMM were employed at $0.25^0 \times 0.25^0$ lat./long. as seen in Fig.1d for comparison. There we see that the strong rainfall zones were radar-detected over the coastal bands in most cases, with the intensity somewhat lower than the automatic records. Where the measured precipitation exceeded 300 mm, the radar-given maximum measurement was lower than 250 mm, suggesting that the radar-located position was relative correct but its measurement was lower compared to automatic records. Since the precipitation measuring radar gave the relatively right site of intense rainfall center so that its measurements could be utilized as reference for the marine rainfall zone and its relative value. Examination of Figs.1a and 1d reveals that the precipitation was imitated over the sea south of 26^{0}N around 122^{0}E, with the intensity higher than radar estimate. Besides, the simulated position and strength of precipitation south of Taiwan were relatively good. As a result, the simulations are basically reliable. The 24-hr coarse mesh (18 km × 18 km) simulated rainfall is quite similar to that from TRMM probings (25km× 25 km) in Fig.1c.

Fig.1 depicts two distinct features of rainfall fields based on observations, TRMM sensings or simulations from the coarse or fine mesh model. One is the noticeable discontinuity arising in the rainbelt to the west of the strongest precipitating center over the land, and the other is the existence of two cores of heavy rain clusters to the north and south of the Taiwan , with rainfall reducing greatly in between. The 1-h simulated precipitation pattern shows that the rainband is continuous prior to July 19/0800 UTC (see Fig.2a) and its breaking happens at model hour 8, followed by increasingly bigger gap (Fig.2b), as clearly revealed on the TRMM image (figure not shown). Why did the rainbelt break in that place and what was the cause for it? We shall deal with the problems in what follows.

Fig.3 gives the typhoon's track (coarse mesh) for 24 hrs around the time of the TC landfall, with its initial position at 0000 UTC, July 19, and the simulated geometry broadly consistent with the observed. The simulation is successful in terms of modelings of the track and precipitation so that the imitations can be employed for analysis to come. Coarse-mesh rainfall was close to TRMM data but there were no *in situ* observations over the sea to validate simulations. The following discussion will be based just on coarse-mesh imitations, unless otherwise mentioned.

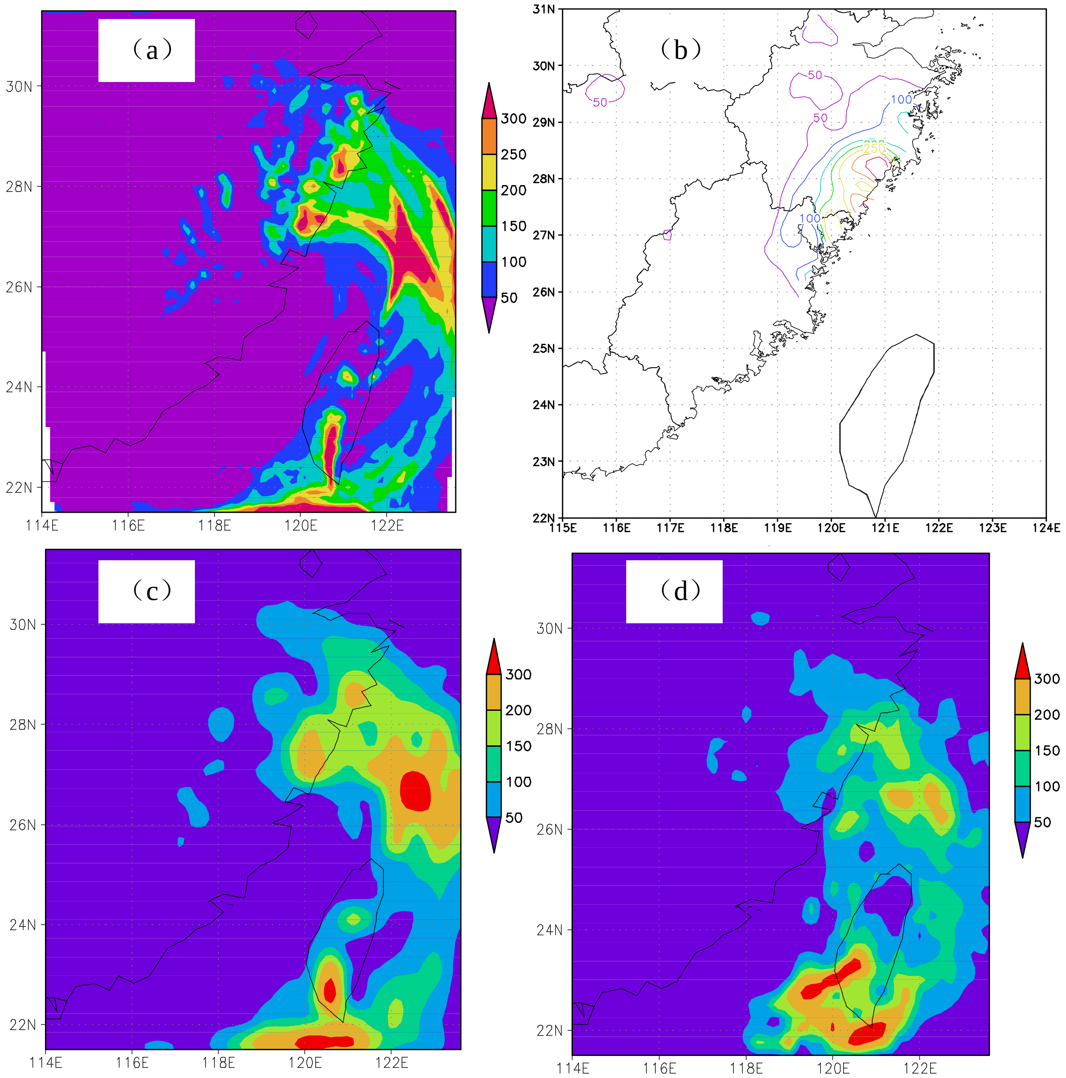

Fig.1. 24-h rainfall (mm) during July 19/0000 to 20/0000 UTC from the fine-mesh emulations in a), observations in b), coarse-mesh simulations in c), and TRMM sensings in d) with the scale beside the diagram denoting the intensity.

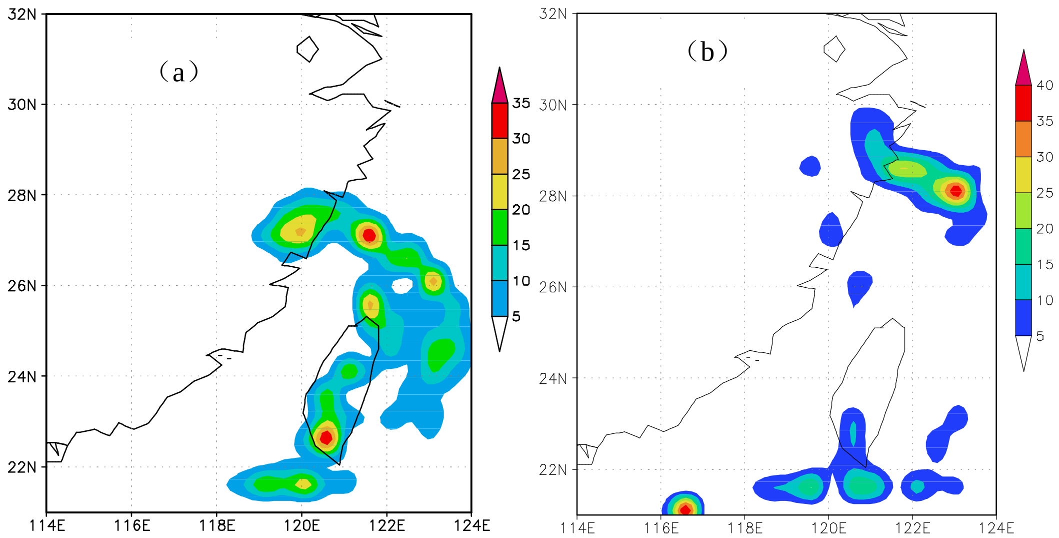

Fig.2. 1-hr rainfall based on 4-h integration in a) and 18-h integration over the coarse mesh in b).

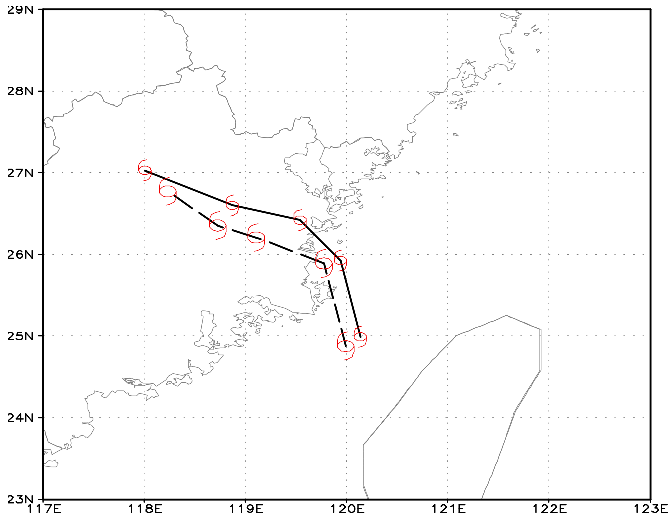

Fig.3. The geometry of the 0505 TC *Haitang* for July 19/0000 ~20/0000 UTC with the simulated (dashed line) in a) and the observed (full line) in b).

4. ANALYSIS OF THE CAUSES OF THE RAINBAND BREAKING

As stated earlier, the rainband experienced breaking around the time of the *Haitang* landfall. The breaking happened mainly in two areas. One distinct breaking was over the sea (~25^{0}N, 123^{0}E) to the east of the TC core, and the other exhibited pronounced discontinuity of rainfall to the west of the strongest typhoon's core over the land (see Fig.1), with the breaking even more clearly revealed on the map of fine-mesh 1-h rainfall (Cf. Fig.9c). The 24-h vorticity variation around 25^{0}N, 123^{0}E (Fig.4a) starting from 0000 UTC, July 19 shows the strongest vorticity at lower levels to be at 0000~0800 model hours, indicating a positive vorticity core around 700 hPa, with weaker negative vorticity above the level; the integration at model hour 9 presents a more intense positive vorticity center at 150 hPa, with the central value in excess of $20\times10^{-5}s^{-1}$, maximizing at $30\times10^{-5}s^{-1}$ at model hour 13 and in contrast, the low-level vigorous vorticity weakened greatly in that period. From model hours 14 to 17 the negative vorticity emerged at 200 hPa while low-level vorticity amplified to some extent. As time went on, the ~200 hPa was largely under the control of vorticity. As seen from the evolution of vertical velocity presented in Fig.4b, although descending appeared in the 200-hPa stronger vorticity zone, ascending remained below 300 hPa that reduced greatly compared to the situation prior to model hour 6, thus revealing that the appearance of vigorous vorticity at 200 hPa led to subsidence, preventing the rising motion from intensification inside the typhoon. It was due to the weakened rising that resulted in the breaking of the rainbelt. As to the formation of 200-hPa vorticity, it will be discussed in the following section.

Examination of 24-hr fine-mesh rainfall (Fig.1a) indicates that precipitation occurred dominantly over the seaboard around the time of landing, and to the west there were banded hyetal zones alone that were evident based on the fine-mesh simulations, with such distinct zones unseen on the map of coarse-mesh emulations. Moreover, to the west there were individual rain clusters, as demonstrated on the TRMM image. Note that the rainband breaking on land differed from that over the sea in that as one of the causes, the hilly seaboard might act as the barrier that gave rise to the breaking. The wind difference (200 minus 850 hPa) showed the shearing of the environmental winds that directed towards the southwest (Fig.9c), where we see most rainbelts were located to the left of the shear line in the downwind direction, a result that agrees well with findings reported by many other writers (DeMaria, 1996; Frank and Ritchie, 1999; Corbosiero and Molinari, 2002). The breaking over the coastal belt may be associated with the unique distribution of the environmental winds, which fails to interpret the distinct breaking over waters and the existence of precipitating areas to the west of the typhoon's center over land, which are the issues to be investigated later. And around the time of landfall, the TC, when approaching land, was coming under the effect of terrestrial systems. Especially its high-level features (e.g., vigor and extent) were much weaker compared to those at low levels, such that midlatitude systems in the higher troposphere have stronger effect on the typhoon. And how did the high-level systems influence the distribution of rainbands and what were the interactions between the typhoon and the systems? These key problems will be examined subsequently.

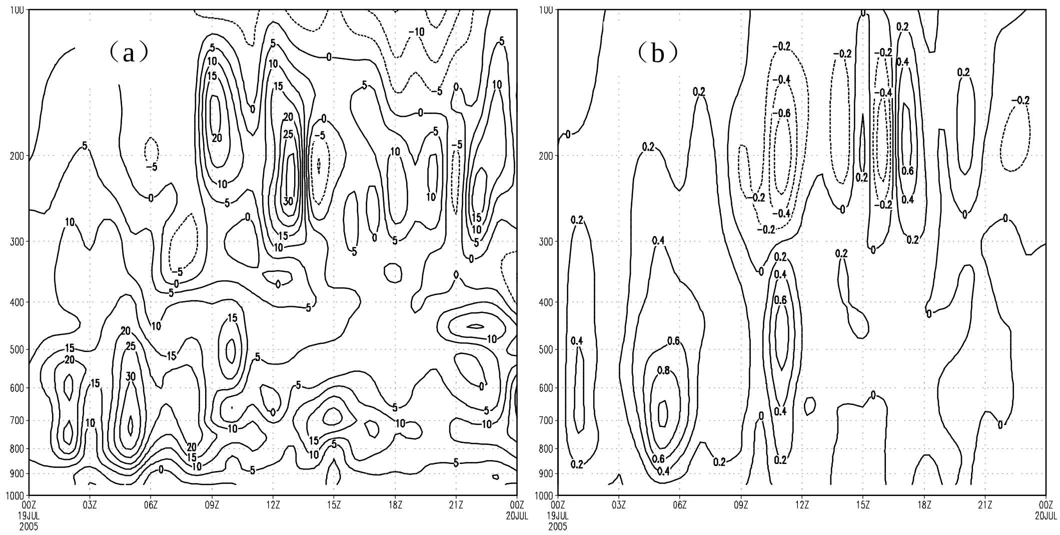

Fig.4. The time–pressure cross section of vorticity ($10^{-5}s^{-1}$) around 25^0N, 123^0E in a), and vertical speed (m/s) in b) for July 19/0000 to 20/0000 UTC.

4.1 The Rainbelt Breaking Associated with Systems at High and Lower Levels

Inspection shows that the 850 hPa convergent flow field matches the 200 hPa divergent field to the east of the TC center (see Figs.5a, b) and to the west the low-level divergence matches the 200-hPa convergence, and particularly the 200 hPa flow field exhibited a northward-extending inverted trough at 0000 UTC, July 19 only that formed by the divergent air combined with flows outside the South Asian high (Fig.6a). As shown by the mean divergence field over 22-30^0N, 111-116^0E on the west side of the typhoon, the lower- divergence is a lot stronger than high-level convergence at model hour 6; at 8-h integration the strongest convergence center emerged at 500 hPa and after model hour 9 the 200 hPa convergence was greatly reinforced, with divergence prevailing at mid – lower levels. It follows that initially divergence dominated low level to the west of the TC center and the 200-hPa convergence began to strengthen after model hour 6, and subsequent to model hour 9 the strongest convergence center emerges at 150 hPa and was maintained there. Inspection of the evolution of 850 hPa circulation (Figs.5a, c) yields that from July 19/0000 to 20/0000 UTC its variation was smaller in sharp contrast to the 200 hPa counterpart, and the inverted trough previously in the outer-region of the typhoon developed a big cyclone with three cores inside (Figs.5b, d), of which core A coincided with the original TC center and cores B and C were cyclonic centers grown to the west of the TC center. Following the compensation principle, the low-level steady divergence favors the formation of a high-level convergence field and cyclonic circulation center, and analysis of the vertical speeds on the west side of the typhoon's core indicates that subsidence is predominant to the west of the TC center (Fig.6b), which is the principal cause of impossibility to beget precipitation over the area.

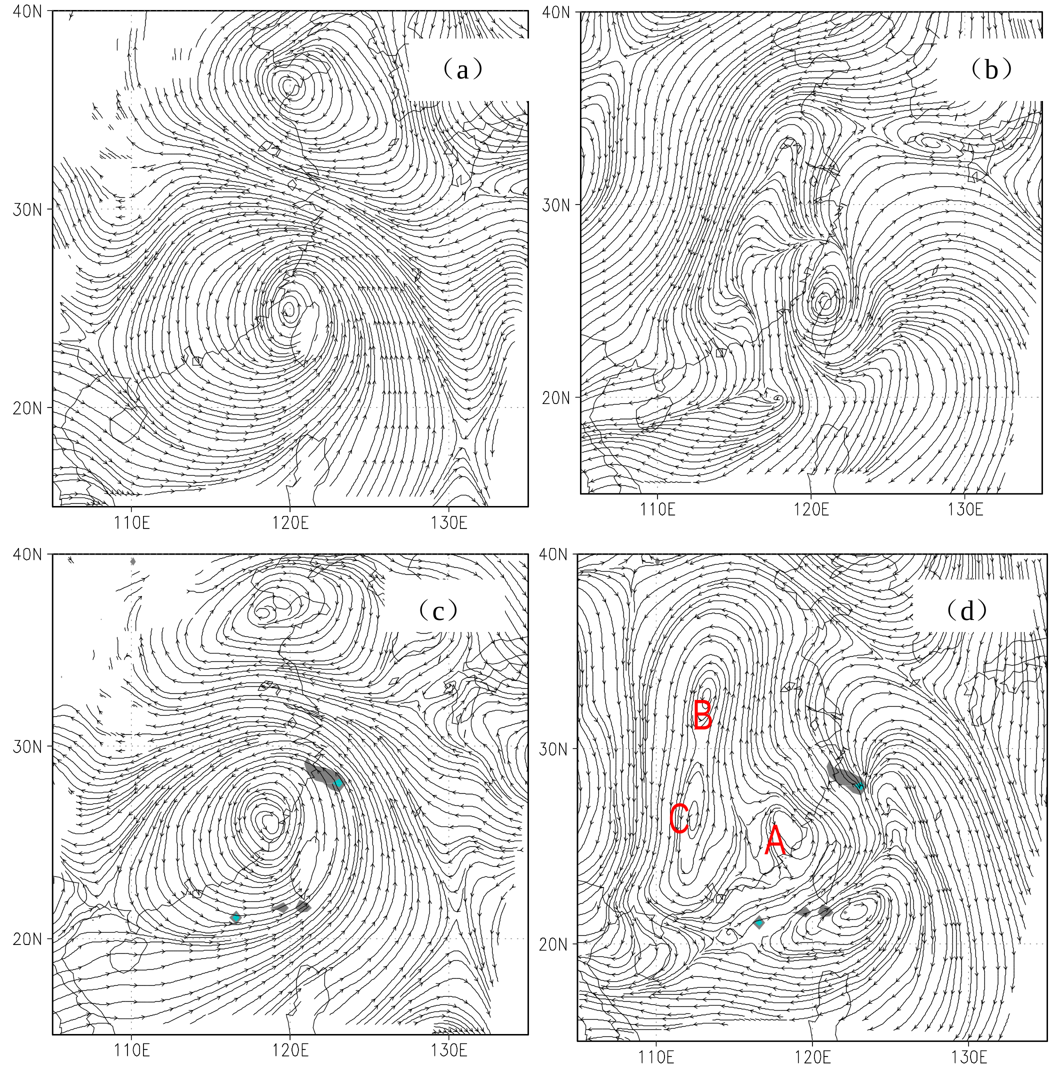

Fig.5. The initial flow field at 850 and 200 hPa, in a) and b) at July 19/0000 UTC and the forecast flow field for 200 and 850 hPa at 0000 UTC, July 20, 2005, in c) and d), respectively, with 1-hr rainfall area shaded.

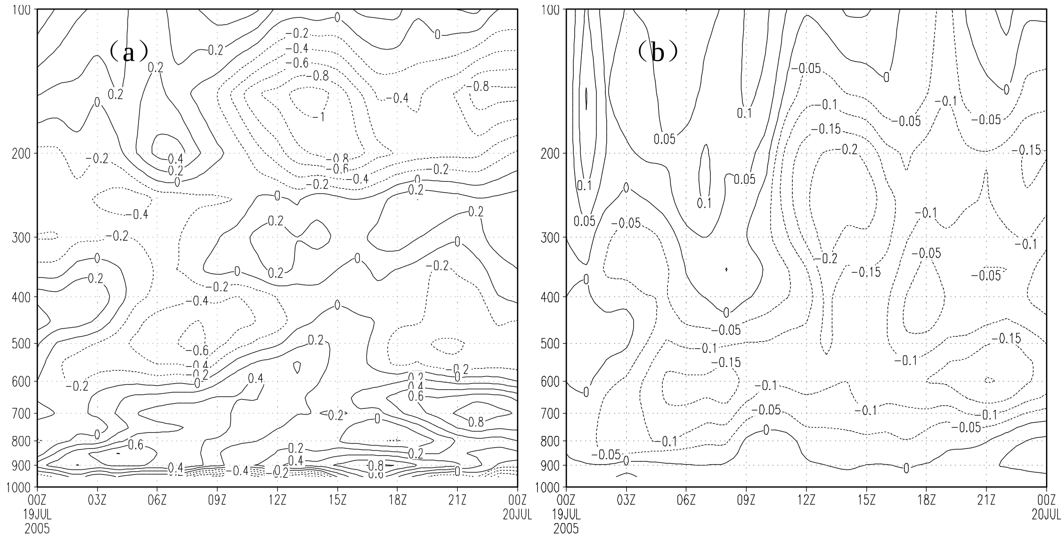

Fig.6. The time–pressure cross section of The divergence field in a) and vertical speeds in b) averaged over 22-30^{0}N, 111-116^{0}E for July 19/0000 to 20/0000 UTC, with the same units as given in Fig.4.

Then, is the development of the 200 hPa cyclonic circulation center related to the spiral rainband breaking over the sea? As shown earlier, the cyclonic circulation formation owing to the gradual amplification of the typhoon after its landfall lies most likely in the existence of divergence field at mid to lower levels to the west of the typhoon. As depicted in Fig.5d, the distinct breaking is seen of the rain zone to the north of Taiwan and over the breaking there is noticeable cyclonic shearing at 200 hPa, where the cyclonic shearing convergence leads to convergent flow subsidence to prevent rainfall formation (Fig.6b). In a consequence, another cause of the breaking is likely to be associated with the cyclonic shearing generated at 200 hPa, a problem that needs to be investigated in the future.

From Fig.7a given circulation and vorticity (1-hr integrations) distributed initially at 200 hPa we see that in the initial field there is a positive vorticity core to the north of the TC center in 35^0N, 117^0E and the positive vorticity zone extends as far as around 22^0N (called region B), with a vigorous positive vorticity center residing over the TC core, which is unrelated to the vorticity zone outside the typhoon, indicating that the TC vorticity field has no relation to midlatitude systems in the initial field, with the rain-forming zone at the brim rather than in the vorticity zone. Afterwards, region-B vorticity develops steadily, with a branch of vorticity migrating southeastward and the TC vorticity spreading outward. At model hour 4 (Fig.7b) the TC vorticity zone connects with region B counterpart, forming a strong positive vorticity passage in 22-25^0N, allowing vorticity outside to come into the TC core on a continuous basis, which is discerned at higher than 400 hPa levels, as given in Fig.8b with a positive vorticity zone in 200-400 hPa, above which the strongest core travels east as a function of time (figure not shown). There are vigorous positive vorticity and wind shear in direction in the pronounced breaking of the rainband to the east of the TC center, which were obviously owing mainly to the steady transfer of midlatitude vorticity. Intense precipitation occurred in the divergent flows at the fringe of the vorticity passage. The vorticity in the TC center shows a trend of spreading outward with airflows in a wavy manner. The vorticity spreading outward from the TC (arrow-denoted) is at the brim of region-B vorticity belt (Fig.7b). At model hour 14 the TC vorticity zone has merged into region-B counterpart that is thus amplified significantly, as even more clearly shown in the time-dependent 33^0N vorticity (Fig.8b). At that time, the cyclonic circulation to the west of the TC got markedly intensified, followed by the TC circulation merging with the midlatitude circulation into a large-scale cyclonic circulation in the higher troposphere when midlatitude positive vorlicity was conveyed stably into the TC circulation (Fig.5d).

Based on the foregoing analysis, we see that around the time of landfall the TC, being close to midlatitudes, interacted with the weather systems there, and at 200 hPa, interactions between the TC circulation and midlatitude system were more strongly, for which the maintenance of 200 hPa positive vorticity passage at midlatitudes allowed vorticity to be transferred into the TC region, thereby making the rainband breaking. No precipitation was formed below the 200- hPa vorticity zone.

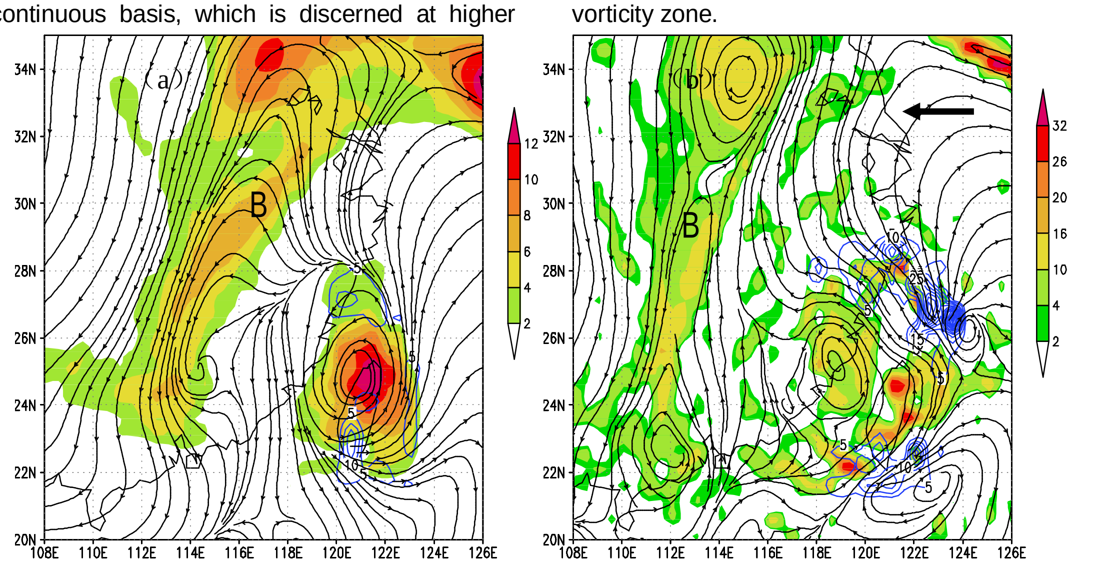

Fig.7. Distribution of positive vorticity ($10^{-5}s^{-1}$) for the circulation field at 1-hr in a) and 12-hr integration in b), with 1-hr isopluvial pointed by arrow at 5 mm intervals.

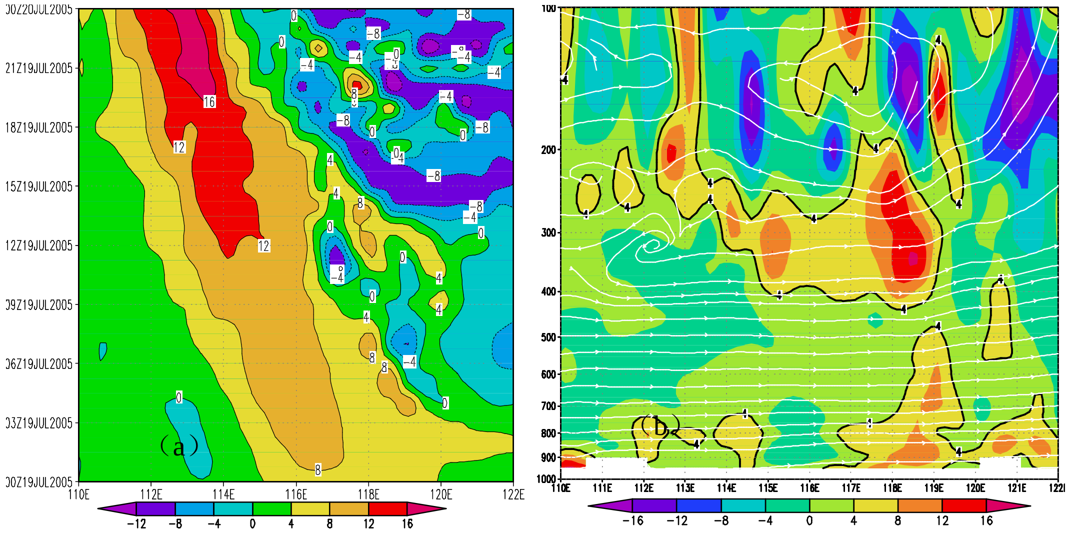

Fig.8. Evolution of 200 hPa vorticity ($10^{-5}s^{-1}$) along 33^0N during July 19/0000 to 20/0000 UTC in a) and the 22^0N cross section of vorticity from 15-hr integration in b).

4.2 Topographic Relation to the Breaking of the Spiral Rainband

To investigate the relation of the topography to the breaking we made a sensitivity experiment with the terrain height reduced below 200 m. Under the assumption of the surface feature in eastern China and northern Taiwan (Fig.9a) we made experiment with 24-h rainfall in comparison to the output of the control run (Fig.1c). It is found the breaking on land remained evident, but with the multiple disturbance rainfall centers no longer available that were originally on the east side of land intense precipitation bands, as clearly seen on the 1-h fine-mesh rainfall map (Figs.9b, c). The marine breaking was still existent, with the 28^0N hyetal zone moved westward over some distance. But from the comparison of total precipitation the breaking bands migrated slightly southward. It follows that the breaking on land and sea remained despite the lowering of the surface features except that the disturbance rainband practically disappeared over the land (Fig.9). Consequently, surface features had greater impact on the disturbance rainbands. With lowered surface features available, the rainfall reduced greatly in intensity over the seaboard, indicating that the original topography played a significant role in augmenting precipitation due to its lifting air. (Zhang et al., 2006; Ji et al., 2007). Analysis also yields that the topography made minor contribution to the breaking.

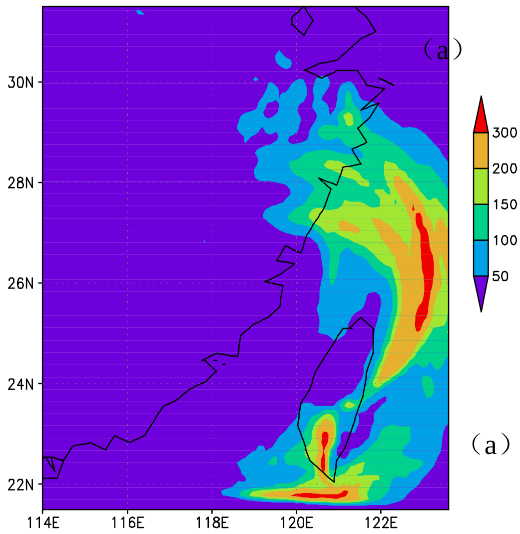

(a)

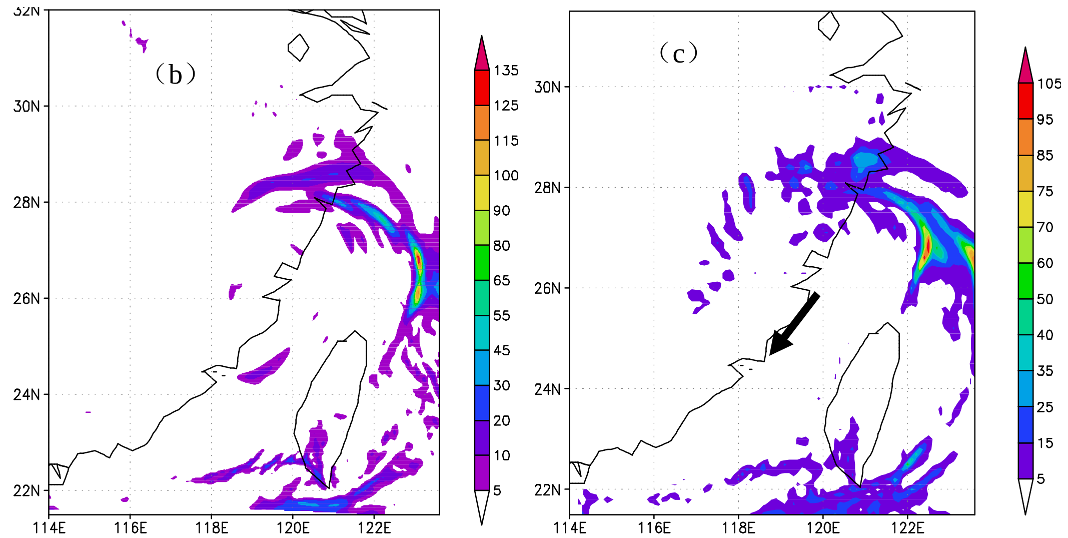

Fig.9. Rainfall from the coarse-mesh reduced-terrain-height sensitivity experiment during July 19/0000 ~ 20/0000 UTC in a), the 12-hr precipitation from the sensitivity run in b) and 12-hr rainfall from the control run in c). Units: mm.

5. CONCLUDING REMARKS

Based on the foregoing analysis, the following points are of note.

1) The reduced-terrain-height sensitivity experiment shows that the topography exerts minor influence on the breaking of rainband. With such surface features adopted the rainbelts extend marginally westward in a less discrete way, indicating that surface features play a greater part in forming land disturbance rainband.

2) The 200-hPa positive vorticity field prevents rainfall from development, with precipitation happening dominantly outside the vorticity zone and interactions between cyclonic flow fields of the typhoon at 200 hPa and midlatitudes have considerable impacts on the breaking of the spiral rainband. Around the time of landfall the mid~low-level divergence fields to the west and northwest of the TC center cause the generation of positive vorticity and cyclonic stream fields at 200 hPa and the vorticity zone rotates counterclockwise with airflows, merging with the TC's vorticity field to form a positive vorlicity passage directed toward the TC, which makes the 200-hPa cyclonic vorticity and wind shear increased to the east of the TC center, accompanied by subsidence that gives rise to the breaking as the main cause of the asymmetric precipitation. The TC's positive vorlicity, when spreading outward as waves, meets and merges with the vorticity zone to the west, causing the cyclonic circulation there to be further amplified and the circulation, when combined with the TC circulation, forms a vigorous 200-hPa cyclonic circulation that is liable for transferring more positive vorlicity into the TC, leading to more evident breaking of the rainbelt.

3) Around the time of landfall, the TC intensity and its influenced extent are much smaller at 200 than 850 hPa so that the 200-hPa TC portion is prone to the effects of midlatitude circulations, especially in eastern Asia where the South Asian high is rather strong at the upper level and influences more greatly the portion of the TC, both interacting to affect the typhoon rainfall more pronouncedly.

REFERENCES

Chen Jiukang and Ding Zhiying, 2000: On a meso rainstorm system from the coupling of high- and low-level jets with the typhoon circulation, *Quarterly J. Appl. Meteor.*, **11** (3), 272-281 (in Chinese).

Chen Lianshou and Meng Zhiyong, 2001: Advances in tropical cyclones in China over the past decade, *Chinese J. Atmos. Sci.*, **25** (3), 420-432 (in Chinese).

Corbosiero, K. L. and J. Molinari, 2002: The effects of vertical wind stress on distribution of conveTCion in tropical cyclones, *Mon. Wea. Rev.*, **130**, 2112-2113.

DeMaria, M., 1996: The effect of vertical shear on tropical cyclone intensity change, *J. Atmos. Sci.*, **53**, 2067-2087.

Frank, W. M. and E. A. Ritchie, 1999: Effects of environmental flow upon tropical cyclone struTCure, *Mon. Wea. Rev.*, **127**, 2044-2061.

Ji Chunxiao, Xue Genyuan, Zhai Fang et al., 2007: Numerical experiment in effects of terrain upon the rainfall structure for typhoon Rananim in its landing, Chinese *J. Atmos. Sci.*, **31** (2), 233-244 (in Chinese).

Nikaidon, Y., 1989: The PJ-like north – south oscillation spectral model T42, *J. Meteor. Soc. Japan*, **67**, 687-704.

Ren Suling, Liu Yimin and Wu Guoxiong, 2007: Numerical study of interactions between the western Pacific subtropical high and typhoon, *Acta Meteor. Sinica*, **65** (3), 329-340 (in Chinese).

Rodgers, Edward B, Jong Jin Baik, Harold F. Pierce, 1996: The environmental influence on tropical cyclone precipitation, *J. Appl. Meteor.*, **33** (5), 573-593.

Sun Jianhua, Qi Linlin and Zhao Siwei, 2006: Study of exceptionally strong rainstorm causing meso convective system in north China associated with typhoon coded as 9608 landing and migrating northward, *Acta Meteor. Sinica,* **64** (1), 57-71 (in Chinese).

Tao Zuyu, Tian Baijun and Huang Wei, 2001: The asymmetric structure and rainstorm for the landing typhoon coded as 9216, *J. Trop. Meteor.*, **10**, 69-77 (in Chinese).

Zhang Jianhai, Chen Hongmei and Chu Xiaoming, 2006: Numerical simulation of topographic impaTCs on the typhoon *Haitang* (coded 0505) during its landfall, *Bulletin of Oceanography*, **25** (2), 1-7 (in Chinese).

Zhu, T., D.-L. Zhang and F. Weng, 2003: Numerical simulation of hurricane Bonnie in 1998. Part I: Eyewall evolution and intensity changes, *Mon. Wea. Rev*., **132**, 225-241.